

Part I

General concepts of PET and PET/CT imaging

Chapter

1

PET and PET/CT physics, instrumentation, and artifacts

Stephen C. Moore and Mi-Ae Park

This chapter provides background material essential for understanding the scientific and technical underpinnings of the image-formation process in positron emission tomography (PET). X-ray computed tomography (CT) will also be briefly discussed, though in much less detail. Instead, we will emphasize, later in this chapter, the ways in which the CT acquisition and resulting images influence reconstructed PET images. Because the terminology used to describe the most important nuclear physics and PET instrumentation concepts may be unfamiliar to some readers, we have highlighted certain key words and expressions in bold font when these terms are first introduced. For more advanced treatments of selected topics related to PET instrumentation and imaging, readers are referred to physics texts, such as those by Cherry *et al.* (1) and Wernick and Aarsvold (2).

Radioactive decay: positron emission, annihilation, and detection

In this section, we discuss the basic nuclear physics concepts on which PET imaging is based. We begin by presenting some information and terminology related to the decay of radioactive atoms, in general, as well as more detailed and specific descriptions of positron decay. Along the way, we will discuss several key characteristics of radioactive nuclei that emit positrons; these will later be shown to influence the quality of PET images.

Radioactive decay

There are many different types of radioactive elements, called **radionuclides**. While all such elements possess **unstable** nuclei, different categories of radioactive elements have been defined according to the manner in which they transform themselves to allow the constituents of the nucleus, i.e., protons and neutrons, to assume a more stable arrangement. When such a transformation occurs, we say that the nucleus has **decayed** from a higher energy, unstable state to a lower energy, more stable state, or often to a fully stable **ground**

state. The total mass-energy of the resulting ground-state atom is less than that of the initial radionuclide. The energy lost by the radioactive nucleus during its decay is normally transferred to one or more particles that are emitted from the atom; thus, it is often possible to determine quite precisely the moment when an unstable nucleus decays, by detecting the emitted radiation using one of several types of radiation detectors. Depending on the **decay mode**, the emitted radiation can consist of charged particles which have mass (e.g., an electron, or a positively charged electron called a **positron**), or particles with zero mass and zero charge (e.g., a **photon**, which is the fundamental particle or “carrier” of electromagnetic radiation). Very commonly, both massive and massless particles are emitted during the decay of a single radioactive atom. The type and number of particles emitted in any given nuclear decay are characteristic properties of the decay mode. Some radioactive elements can decay by more than one possible mode.

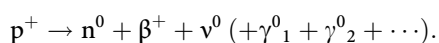
Each nucleus can be uniquely characterized by an **atomic number, Z**, and a **mass number, A**, where Z is the number of protons in the nucleus, and A is the sum of the number of protons and neutrons in the nucleus. Stable nuclei generally have approximately the same number of protons and neutrons (or somewhat more neutrons than protons), whereas unstable nuclei usually have an excess number of protons or neutrons. Two or more radionuclides which have the same number of protons, but a different number of neutrons within their nuclei are called **radioisotopes** of the same element. For example, iodine-123, iodine-125, and iodine-131 are all radioisotopes. There are several unique properties of every radionuclide; these include the nuclide’s decay mode (or combination of modes), its decay **transition energy** (which is divided among the resulting decay particles), and its **half-life**, which is the time required for half of the initial number of radioactive nuclei in a sample to decay. While we can never predict the exact moment in time when a given nucleus will decay, or – for multiple, or complex decay modes – the exact decay mode or the exact energy of each of the possible emitted particles, we do know these properties quite well in a statistical sense. In fact,

Part I: General concepts of PET and PET/CT imaging

the phenomenon of radioactive decay can be described as a so-called Poisson statistical process and, for any given radionuclide, we can state with a high degree of certainty the *average* time required for a large number of such radioactive nuclei to be reduced by one-half (i.e., the radionuclide's half-life). Similarly, we can reliably predict the average number of emitted particles of any given type, as well as the distribution of their energies.

Positron decay

Unstable nuclei possessing an excess number of protons often become more stable by undergoing **positron decay**. (This is also sometimes referred to as positive **beta decay**, because positrons or electrons emitted from a nucleus during a radioactive decay are commonly called positive or negative **beta particles**.) During positron decay, a positively charged proton in the nucleus (p^+) appears to change into a neutral (zero-charge) neutron (n^0) while, simultaneously, a positron (β^+) is emitted from the nucleus, along with a zero-mass, neutral particle called a neutrino (ν^0). Because a proton, essentially, turns into a neutron during the decay, the initial element is transformed into another element whose atomic number, Z , is reduced by one, but whose mass number, A , remains unchanged. Sometimes, following positron decay, the nucleus will end up with an appropriate ratio of protons to neutrons to be stable; however, the combined properties of all of the nuclear constituents may still not result in a fully stable state, in which case the nucleus is said to be in a **metastable state**. When this occurs, the metastable nucleus generally decays further to the ground state by rearranging its nuclear constituents and emitting one or more photons in the process. (When photons are emitted from a nucleus, they are referred to as **gamma radiation**.) Positron or β^+ decay (including, for some radionuclides, one or more possible neutral gamma photons, γ^0) can thus be summarized symbolically by the formula:



Note that the total electrical charge is conserved in this decay process, as it must be. The left-hand side of the equation shows a proton with a single positive charge (+1), and the sum of the charges of all particles on the right-hand side is also +1.

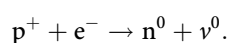
Positron emitters used in biomedical imaging

It can be seen from this formula that the transition energy associated with a *pure* positron decay (with no accompanying gamma photons) is shared among three particles: a neutron which remains bound within the nucleus, a positron, and a neutrino. Because there are three decay particles which share the nuclear transition energy, the kinetic energy of the emitted positron is not restricted to a single value but, instead, is characterized by a continuous **energy spectrum**, ranging from zero up to some maximum value, $E_{\beta, \max}$, which is different for each different radionuclide. The average positron energy is, typically, about one-third of $E_{\beta, \max}$.

Most positron emitters used for biomedical imaging applications have relatively short half-lives, ranging from seconds to minutes, although there are exceptions. Examples of commonly used radioactive elements which decay by positron emission (and their half-lives) include fluorine-18 (^{18}F ; $T_{1/2} = 110$ min.), carbon-11 (^{11}C ; $T_{1/2} = 20$ min.), nitrogen-13 (^{13}N ; $T_{1/2} = 10$ min.), oxygen-15 (^{15}O ; $T_{1/2} = 122$ s), and rubidium-82 (^{82}Rb ; $T_{1/2} = 75$ s). Some of these positron emitters, e.g., ^{11}C , ^{13}N , ^{15}O , are radioisotopes of corresponding stable elements (^{12}C , ^{14}N , ^{16}O) that are ubiquitous throughout all biologic systems. This affords the opportunity to radiolabel many different bio-molecules of interest simply by replacing a stable element in the molecule with the corresponding positron-emitting isotope. The stable isotopes corresponding to other positron emitters, such as ^{18}F and ^{82}Rb are found less commonly in living systems; however, some of these radionuclides can still be used to label various analogs of bio-molecules, e.g., the glucose analog, ^{18}F -fluorodeoxyglucose (FDG), while others can be used in the form of radioactive salts, e.g., ^{82}Rb -chloride, which behaves as a potassium analog *in vivo*.

Electron capture

It is important to note that not all positron emitters decay solely by β^+ decay; some unstable radionuclides characterized by an excess number of protons can also decay by a competing process, known as **electron capture**, in which an inner-shell atomic electron is captured by the nucleus, where it combines with a proton and, effectively, changes into a neutron. Just as for β^+ -decay, a neutrino is produced during electron capture, although no positron results from this decay mode:



Carbon-11 is an example of a radionuclide which decays either by positron emission (in 97% of decays), or by electron capture (in 3% of decays). Clearly, if a positron emitter decays much more frequently by electron capture, then this radionuclide would probably not be very useful for PET imaging, since its positron yield per nuclear decay would be very low.

Positron annihilation

In positron emission tomography, the positrons themselves are not directly detected to form images. This is because positrons have a short range in tissue (less than a few millimeters), which means that almost none of them will escape the patient's body to be detected. After an emitted positron loses most of its kinetic energy, by scattering off of multiple electrons along its path, it combines with a nearby electron to form an atomic-like species known as **positronium**. This extremely short-lived state promptly results in the annihilation of the positron and electron to produce two photons which are emitted back-to-back in opposite directions. (See Figure 1.1.) Both of the **annihilation photons** have the same energy – 511 thousand (kilo) electron volts (keV) – which is the rest-mass energy of

Chapter 1: PET and PET/CT physics, instrumentation, and artifacts

the electron and the positron from which the photons originated. To be used for PET image formation, both of these photons must escape the patient and then be detected simultaneously in two of the many thousands of PET detectors which encircle the patient in a modern PET scanner. It should be mentioned that the neutrino emitted during β^+ decay is almost impossible to detect because neutrinos only interact in matter with extremely low probability. Although they do not play a direct role in the PET image-formation process, neutrinos do influence the energy spectrum and range of the positrons with which they share the energy made available in the decay process.

The PET measurement process

A schematic view of a PET detector ring is shown in Figure 1.2A, along with an illustration of a single positron-annihilation event occurring within a patient's body, and the resulting two 511-keV annihilation photons being detected in coincidence in two opposing detectors. The path along which the back-to-back annihilation photons travel is defined by the two detectors in

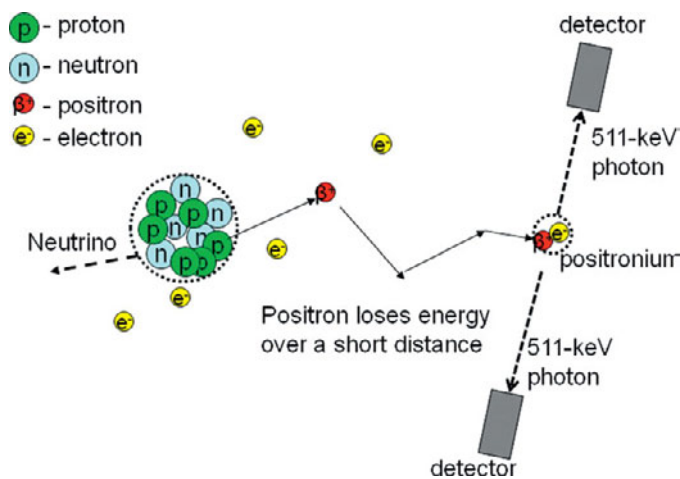


Figure 1.1 Positron decay and annihilation. The emitted positron travels a distance of up to several millimeters, depending on its initial energy (Table 1.1). After losing energy by multiple scatter interactions, the positron and an electron annihilate to form two 511-keV photons, emitted in opposite directions.

which the photons are detected. This path is often called a PET **line-of-response**, or **LOR**. Because all of the detectors are electronically placed in coincidence with all other detectors within an arc on the other side of the patient, it is easy to see there are a great many possible LORs in a PET scanner. As each coincidence-pair event is detected in the PET scanner, the system electronics computes the unique LOR associated with the two detectors which “fired.” Each LOR is mapped to a unique location in a computer memory, which is incremented every time an event is detected along the corresponding LOR.

Figure 1.2B shows only those LORs which connect a single detector to all the detectors on the other side of the patient. During the acquisition of PET data, certain LORs will record more decay events, while others will record fewer events, depending on the distribution of radioactivity within the patient's body. At the end of the PET acquisition, each LOR will have recorded a total number of counts proportional to the *integral* of the radioactivity concentration along that LOR. It is clear from Figure 1.2B that the pattern of all LORs involving a single detector resembles a “fan” of LORs across the patient. In fact, we often refer to this data format as **fan-beam projection data**. All of the other detectors around the ring will also have their own coincidence fans of data. Given a complete set of such angular projection data, which includes fan-beam projections from all angles around the PET detector ring, it is possible to reconstruct an image corresponding to the concentration of the positron-emitting radionuclide within a transaxial “slice” through the patient's body. For those readers who are already knowledgeable about X-ray CT, the fan-beam projection concept should be quite familiar. In CT, the scanner records fan-beam projections connecting each X-ray source position, i.e., during the rotation of an X-ray tube, to all opposing detectors. In CT, each projection-ray is a measurement of the integral of the so-called **linear attenuation coefficient** along the line, whereas in PET, each projection ray is proportional to the integral of the radiotracer's activity concentration along the LOR. Therefore, the image intensity (brightness) in a given region of a reconstructed CT image is proportional to the region's linear attenuation coefficient (related to the region's density and the effective atomic

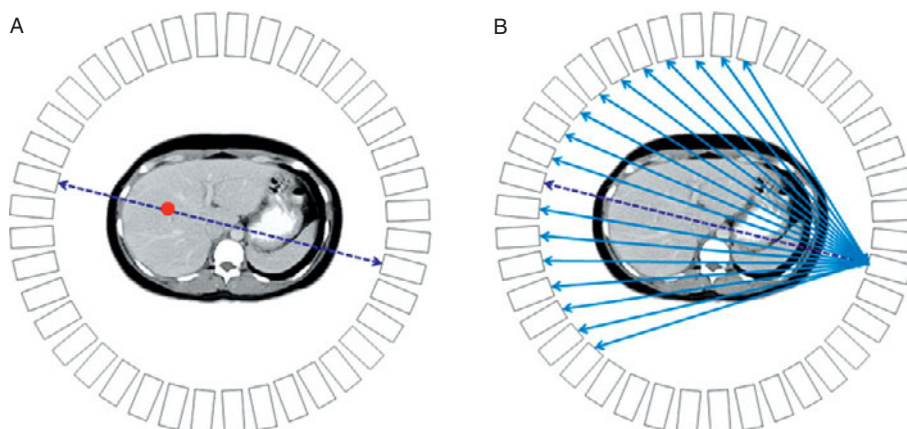


Figure 1.2 (A) A single coincidence line-of-response (LOR) defined by two detector elements; (B) a fan-beam projection of coincidence LORs, shown superimposed on a X-ray CT transaxial section through the abdomen.

Part I: General concepts of PET and PET/CT imaging

number of the material), whereas the local image intensity in reconstructed PET images is proportional to the concentration of radioactivity in the region in units of decays per second per mL (Bq/mL), or $\mu\text{Ci/mL}$ (where $1 \mu\text{Ci} = 37 \text{ kBq}$).

The earliest PET tomographs consisted of a single ring of detectors; these systems acquired and reconstructed data from a single transaxial section of the patient at one time. To image additional “slices” required stepping the patient table through the PET scanner, and acquiring another set of coincidence projections at each additional desired axial slice location. Modern PET scanners have many more rings of detectors surrounding the patient, which permit more slices within a larger axial range (typically 15–20 cm) to be imaged simultaneously.

Spatial resolution of PET images

The spatial resolution of an imaging system determines our ability to resolve two distinct features that are close together in the patient being imaged. A system with good spatial resolution will allow us to visually discriminate the two features when they are very close together, whereas a system with poor resolution will only permit us to resolve the features when they are farther apart. Spatial resolution is often described by a single number representing the **full-width-at-half-maximum (FWHM)** of the so-called **point-spread function (PSF)**. If a very tiny point-source of radioactivity is imaged in a PET scanner, then the PSF is just the blurred image of this source. The FWHM of the PSF is simply a measure of the extent or width of the blurred PSF at the location corresponding to half of the maximum image brightness within the point. The FWHM is also a convenient measure because it also provides an indication of the distance of separation between two point sources at which they would blur together, and no longer be resolvable as two separate sources. In PET imaging, the spatial resolution is primarily affected by the following factors: detector size, positron range, photon non-colinearity, and image reconstruction. These factors will now be discussed, one by one.

Detector size

The effective width of the lines-of-response connecting any pair of detectors is obviously affected by the size of the detectors themselves; the use of smaller detectors implies that the LOR connecting them will be “narrower,” i.e., its width will be known more precisely, whereas wider detectors will lead to a greater uncertainty in our ability to localize annihilation events, with a concomitant deterioration of spatial resolution. As shown in Figure 1.3, the FWHM of the LOR is not constant everywhere; since two detectors must simultaneously detect both coincident photons, the detector resolution varies along the LOR. It turns out that the detector PSF is approximately triangular in shape at the mid-point between the two detectors, where the detector resolution, R , is best and the FWHM is equal to half the detector size, d . The detector PSF becomes increasingly wider for annihilation events located closer to

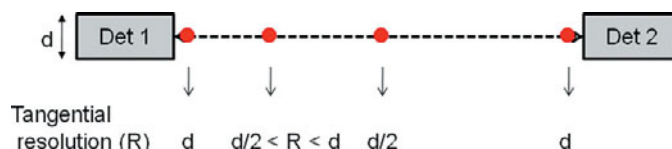


Figure 1.3 Detector resolution, R , depends on the width of a detector element, d , perpendicular to the LOR, and varies with the source location along the LOR. The detector element size, d , is typically several millimeters in most PET scanners.

either of the two detectors; the worst detector resolution is found immediately adjacent to a detector, where the PSF shape is approximately rectangular with a FWHM of the detector PSF equal to the detector size.

These considerations imply that a large number of very small detectors should be used in PET scanners; however, there are other important factors which must be considered when designing a PET system. Importantly, the detectors are often the most expensive components in the scanner, so a large increase in the number of detectors may not be possible. Another consideration is that there is always a small gap between detector elements. This implies that a system containing a larger number of smaller detectors will have a greater percentage of “dead-space” between detectors, which decreases the overall detection efficiency of the scanner. Finally, when more detector elements are used in a system, it becomes more difficult to identify accurately the exact detector element in which a photon interaction occurred.

Positron range

Ideally, we would like each positron-decay event to be located along a well-defined LOR in the PET scanner. Unfortunately, however, as shown in Figure 1.1, the positron can sometimes travel through a distance up to several millimeters away from its point of origin, before annihilating with an electron to produce the back-to-back photons which define the LOR associated with the event. Because the positron’s path through the surrounding materials can be quite tortuous, owing to multiple scattering, this means that, in some cases, a positron might end up back near its origin before it loses enough energy to annihilate. In this case, there would be very little loss of spatial information because the annihilation would occur close to the point of nuclear decay. However, on average, most positrons are located somewhat farther from their point-of-origin when they annihilate. The maximum possible energy of the emitted positrons, their average energy, and the root-mean-square (rms) position deviation from the location of the positron decays are listed in Table 1.1 for a variety of common positron emitters. (Beta-particle energy values are shown in units of millions of electron volts, MeV.)

Photon non-colinearity

The positron and electron which comprise the short-lived positronium “atom” both have some (generally small) kinetic energy and momentum before they annihilate to produce

Table 1.1 Properties of some positron emitters.

Radionuclide	E_{\max} (MeV)	E_{ave} (MeV)	RMS position deviation in water (mm)
^{11}C	0.96	0.38	0.42
^{13}N	1.19	0.49	0.57
^{15}O	1.72	0.73	1.02
^{18}F	0.64	0.24	0.23
^{82}Rb	3.35	1.52	2.60

back-to-back photons. If their combined momentum before the annihilation had a significant component in a direction perpendicular to the direction along which the annihilation photons are emitted, then, because each vector component of momentum must be conserved, it turns out that the angle between the annihilation photons will not always be exactly 180 degrees but, instead, will deviate slightly from 180 degrees from event to event. Since the LOR is defined by the straight line connecting the two detectors which sense the annihilation photons, it can be seen from Figure 1.4 that any non-colinearity in the directions of the two annihilation photons will introduce an additional uncertainty in the determination of the event location. Because this effect produces an *angular* deviation, the magnitude of the position uncertainty arising from photon non-colinearity increases with the diameter of the PET scanner's detector ring. The resolution attributable to photon non-colinearity has been shown (3) to be well approximated by the following empirical function of ring diameter, in centimeters:

$$\text{FWHM}_{\text{non-col}}(\text{cm}) \sim 0.0022 \times \text{ring diameter}(\text{cm}).$$

Thus, for a whole-body PET scanner with a ring-diameter of 90 cm, the FWHM resolution attributable to non-colinearity is approximately 2 mm.

System resolution and reconstructed resolution

The FWHM of the overall system resolution can be approximated fairly well as the quadrature sum (i.e., the square-root of the sum of squares) of the various contributing factors:

$$\text{FWHM}_{\text{sys}} = \sqrt{\text{FWHM}_{\text{det}}^2 + \text{rms}_{\text{range}}^2 + \text{FWHM}_{\text{non-col}}^2}.$$

For a PET system with 4.2-mm wide detectors and a ring-diameter of 90 cm, the resolution near the center of the scanner is thus expected to be ~ 2.9 mm when imaging F-18, whereas if the same system is used to image Rb-82, the system resolution is ~ 3.9 mm.

So far, we have only discussed those factors contributing to the overall system resolution which are limited by the fundamental physics of positron decay and annihilation, as well as by the “hardware” design of the PET tomograph. It is important to realize, however, that the resolution of the final

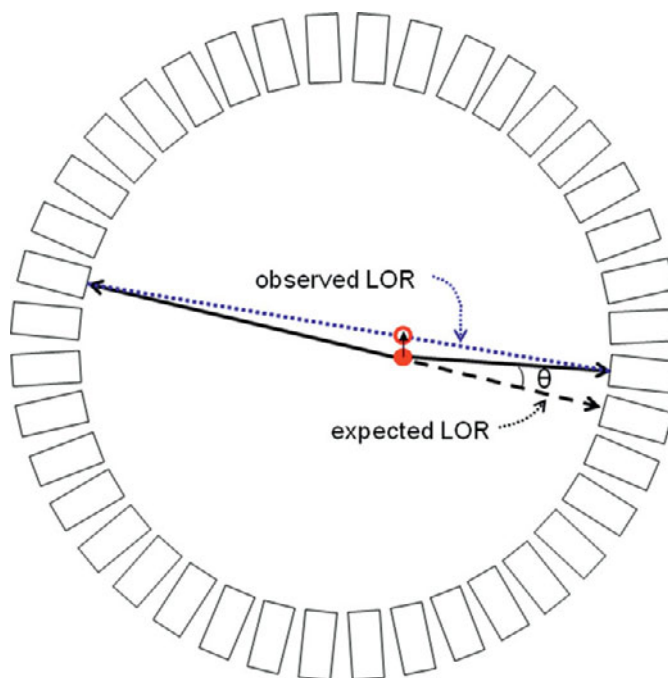


Figure 1.4 Resolution degradation arising from non-colinearity in the directions of the two 511-keV annihilation photons.

PET images will also be influenced by the type of tomographic reconstruction algorithm (e.g., filtered-backprojection, iterative maximum-likelihood, etc.), as well as by the user's choice of reconstruction parameters, which generally affect the “tradeoff” between reconstructed image resolution and image noise. Because the choice of reconstruction method and parameters often depends strongly on the type of PET study being performed, there is a rather wide range of reconstructed resolution values utilized in clinical practice.

Detector depth-of-interaction effect on spatial resolution

As seen in Figure 1.5, when considering the detector spatial resolution perpendicular to LORs located at larger radial distances from the center of the PET scanner, there is an additional degrading factor which can be attributed to a lack of knowledge about the depth within each detector where the photon interaction occurred. For LORs near the center of the PET scanner, we also have no knowledge of the **depth-of-interaction (DOI)** in the detectors; however, the DOI effect only degrades spatial resolution significantly for LORs at large radial offsets, where the DOI uncertainty, essentially, makes the detectors appear to be wider than they actually are. The worse resolution attributable to this effect could be improved by using thinner detectors; however, this can be counter-productive because thinner detectors will significantly reduce the scanner's detection efficiency. Another (expensive) approach to reduce the influence of the detector DOI effect is to utilize two layers of independent detector elements, without reducing

Part I: General concepts of PET and PET/CT imaging

the total thickness of the detectors. For this method to work, the system must be able to determine which of the two detector layers detected the photon interaction; there are various ways of doing this (4), but these are beyond the scope of this chapter.

PET detectors and system geometry; 2-D and 3-D imaging modes; random- and scatter-coincidence events

PET detectors

The detectors used in most PET scanners are made from high-density inorganic scintillation crystals, coupled to photomultiplier tubes. The purpose of the photomultiplier tubes is to detect a pulse

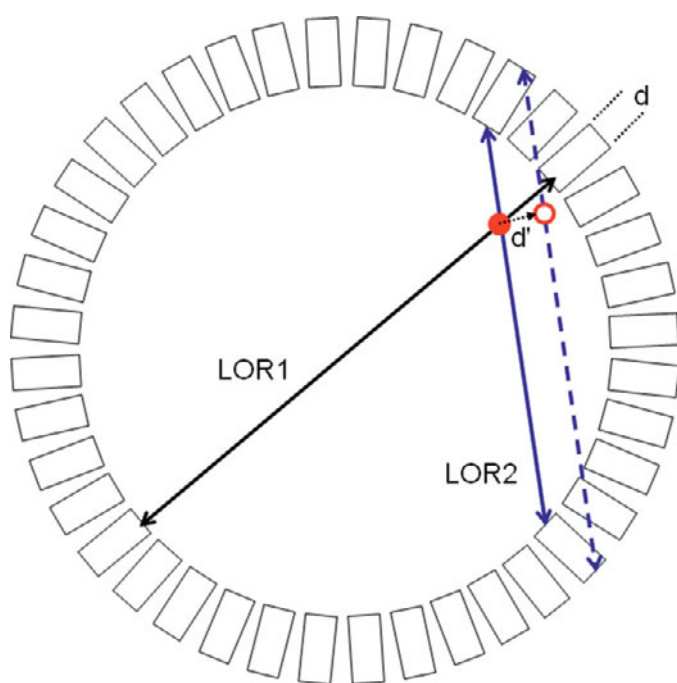


Figure 1.5 The apparent width, d' , of LOR 2 – located at a large radial distance from the center of the scanner – is increased by uncertainty in the detector depth-of-interaction (DOI), whereas the width, d , of the more centrally located LOR 1 is relatively unaffected by DOI uncertainty.

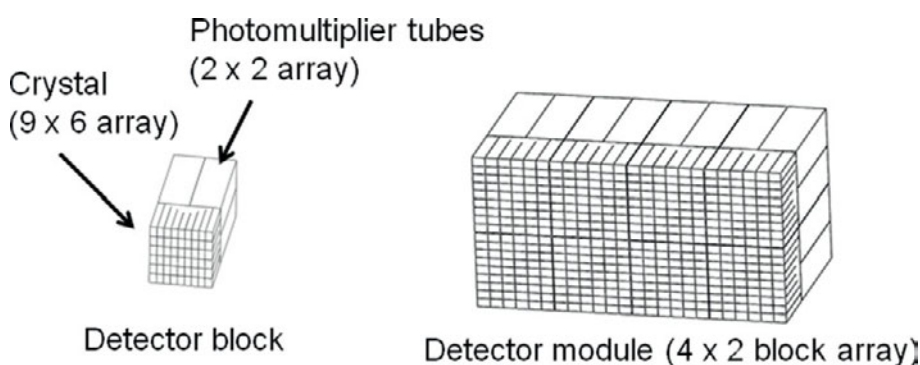


Figure 1.6 Illustration of a PET detector block (left) and module (right). Crystal element dimensions typically range from 4 to 6 mm in cross-section, and 20 to 30 mm in depth.

of light created in one or more scintillation crystals when an incident annihilation photon undergoes an interaction. As discussed above, to obtain good spatial resolution, the individual detector crystals should be very small in cross-section (e.g., 4.2×6.3 mm), but they must be thick enough (e.g., 20 to 30 mm deep) to stop most of the 511-keV photons entering the crystal. In most PET scanners, the individual crystal elements are organized into **detector blocks** (Figure 1.6), viewed by a 2×2 array of photomultiplier tubes (5). The blocks are usually fabricated from a single large rectangular crystal, into which relatively deep grooves are cut to segment the block into individual crystal elements. Regardless of whether grooved blocks or individual discrete elements are used, however, each element should be optically isolated to some extent from its neighboring crystal elements, to reduce the light cross-talk from one crystal element to others within the block. This is often accomplished by coating the surfaces of each element with an opaque, light-reflecting layer. In actuality, as described below, a small amount of light spreading within the block is necessary for determining the exact crystal in which an incident annihilation photon interacted.

When a photon from a positron–electron annihilation interacts in a scintillation crystal, a flash of visible light photons is created within a very small region surrounding the interaction point. The intensity or brightness of this flash, i.e., the number of light photons generated, is linearly proportional to the total energy deposited in the crystal during the annihilation photon's interaction. The number of light photons emitted per unit time after the initial interaction can generally be described by a rapid exponential or bi-exponential decay. Most of the time, one of two types of interactions will occur in the crystal: either photoelectric absorption or Compton scattering of the incident photon. If a 511-keV photon's energy is fully absorbed, e.g., by a photoelectric interaction in the scintillation crystal, then the number of visible light photons created in the crystal will be greater than the number of light photons generated by an annihilation photon undergoing a Compton-scatter interaction in the crystal, since the scattered photon carries some of the energy away from the initial interaction point. The scattered photon might then interact again in either the same or a different detector element, or it could escape the detector material altogether. Clearly,

Chapter 1: PET and PET/CT physics, instrumentation, and artifacts

photoelectric interactions are preferable because more energy is deposited at the first interaction point and more scintillation light is produced in comparison to a Compton interaction.

Because the grooves in the crystal block are cut less deep in the center of the block than near the edges, the light from an interaction in the central crystal elements will spread out more over the four photomultiplier tubes, in comparison with the light from an interaction in one of the corner crystals. The crystal where the interaction took place can usually be identified quite accurately by calculating (in the detector block's electronics) two appropriate linear combinations of the photomultiplier tube signals, one for the crystal's horizontal location and the other for its vertical location (e.g., Figure 1.6), and dividing by the total energy deposited in this event, which is, essentially, the sum of the light signals from all four photomultiplier tubes.

Based on the considerations described above, we are now in a position to summarize the most important physical attributes of scintillation-detector materials used for PET imaging. The best scintillators clearly need to be fast and bright, but they should also have a high stopping power (linear attenuation coefficient), and a high **photofraction** (percentage of photoelectric, as opposed to Compton or other interactions). In addition, the wavelength of the visible light produced in the scintillator should be reasonably well matched to the spectral sensitivity of the photomultiplier tubes used to detect the light. **Fast scintillators** are those in which the light flash takes place almost immediately after the annihilation-photon interacts in the crystal, so that the system can determine if a coincident photon was detected at almost the same time in some other detector on the other side of the PET scanner. A **coincidence timing window** width ranging from somewhere between 6 and 12 nanoseconds is used to define coincidence events in most PET systems today. An equally important consideration, however, is that the light pulse must decay very rapidly, so that the detector block will be ready to accept and process the next event as soon as possible.

Bright scintillators produce enough light with each interaction to permit unambiguous identification of the crystal in which the interaction took place; if too few light photons are available for the event position calculation, then there could be a large uncertainty in determining the crystal of interaction, which degrades spatial resolution. Furthermore, the total energy of the detected photon would also not be known with good precision if too few light photons are produced per event. The energy information is useful for reducing the number of detected photons which have scattered too many times in either the patient or the detector, or both. This is accomplished electronically by using a **pulse-height discriminator** to reject events producing light signals that are either too low (too few light photons) or too high (too many light photons). Events detected with too much energy occasionally occur when two or more photons from two different decays are detected in the same detector block at almost the same time.

Table 1.2 Some properties of scintillation crystals.

Property	NaI(Tl)	BGO	LSO	LaBr ₃
Density (g/mL)	3.67	7.1	7.4	5.3
Effective Z	51	75	66	47
Attenuation length at 511 keV (cm)	2.91	1.04	1.14	2.13
Decay time (ns)	230	300	40	35
Light photons/MeV	41 000	9000	26 000	61 000

Good scintillator materials for PET should also have a high **stopping power** at 511 keV. The stopping power is directly related to the linear attenuation coefficient, which implies that the detectors should have a high effective atomic number, as well as a high physical density. In this case, the detector material's attenuation length – which is the inverse of its linear attenuation coefficient at 511-keV – would be short enough that most annihilation photons would interact within a 2- to 3-cm-thick crystal. Furthermore, the photofraction should also be as high as possible, since more energy is deposited in the crystal during photoelectric interactions, in comparison with Compton-scatter interactions. Finally, if a 511-keV photon scatters in one crystal element, but then deposits most of its energy in some other crystal in the same detector block, this could also introduce an error in the LOR associated with the event.

The properties of a few standard scintillators used in nuclear medicine applications are shown in Table 1.2. (For additional properties, the reader is referred to reference (6).) It can be seen that thallium-doped sodium-iodide, NaI(Tl), which is used in most gamma cameras for lower energy single-photon nuclear medicine imaging, has a significantly lower effective atomic number and density than those of bismuth germanate (BGO) and lutetium oxyorthosilicate (LSO), which are used in most PET scanners today. Because of its low stopping power or, equivalently, its longer attenuation length at 511 keV, NaI(Tl) is not often used for PET imaging, despite its reasonably fast light decay time and relatively high total photon yield per MeV of energy deposited during the interaction of the annihilation photon. Among the more commonly used PET scintillators, BGO has better stopping power than LSO; however, LSO is significantly faster and brighter than BGO. Lanthanum bromide, (LaBr₃) despite its longer attenuation length than LSO, is faster and brighter than LSO; for this reason, lanthanum bromide may be better suited than LSO for use in specialized **time-of-flight** PET systems (7), in which the location of the point where the positron annihilated is estimated using the photon arrival-time difference of the two detectors which define the LOR.

PET scanner geometry and acquisition modes

There are two different ways of acquiring data in detector-ring-based PET systems. In the so-called two-dimensional

Part I: General concepts of PET and PET/CT imaging

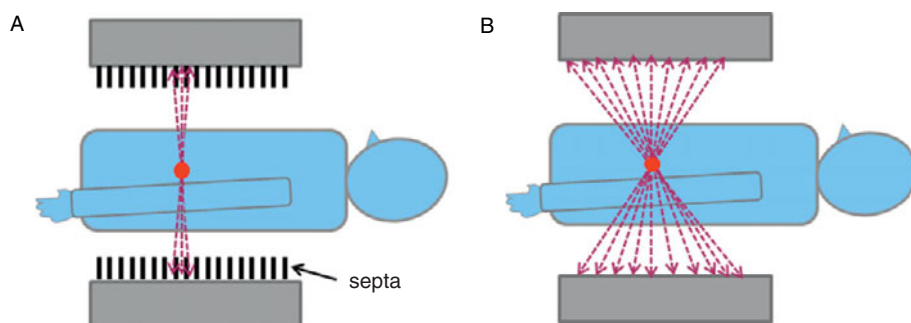


Figure 1.7 PET data acquisition modes: (A) 2-D; (B) 3-D.

(2-D) mode, LORs are acquired in a slice-by-slice manner; in other words, coincidence events are only allowed between detector crystals located within the same axial ring of detectors or, in some cases, among detectors in two or three adjacent detector rings. In this mode, potential coincidence events between detectors located farther apart in the axial direction are limited further through the use of annular septa, made from tungsten or lead, which physically restrict the axial acceptance angle for possible coincidence events by attenuating photons traveling towards the detector ring at larger angles of incidence (e.g., Figure 1.7A). In three-dimensional (3-D) data-acquisition mode, the axial collimator septa are removed from the scanner, and coincidence events between detectors located in more widely separated detector rings are also included as valid events (Figure 1.7B). Obviously, 3-D mode allows many more valid coincidence LORs than 2-D mode, so a PET scanner's count sensitivity is typically about 6–10 times higher in 3-D mode than in 2-D mode. In recent years, there has been a clear increase in the use of 3-D-mode scanning (8), for reasons described below.

Some PET systems are still manufactured with both 2-D and 3-D mode data-acquisition capability; such scanners have retractable annular septa which are positioned appropriately within the scanner for 2-D-mode scanning, but can be quickly and automatically moved out of the scanner for 3-D-mode acquisitions. Other manufacturers are now selling PET scanners which can only acquire data in 3-D mode. Because the photon flux hitting the detector crystals is much higher in 3-D than in 2-D mode when the axial collimators are present, PET scanners based on fast scintillator crystals, such as LSO, may be somewhat more useful for 3-D-mode scanning than systems with slower crystals. Nevertheless, very good-quality 3-D scans are also being routinely acquired today with slower BGO-based scanners. While the detectors in each ring could, in principle, be placed in coincidence with detectors in all other axial rings, in practice, the manufacturers often specify some **maximum acceptable ring difference** which is less than the total number of detector rings in the system.

For 3-D-mode imaging, the PET system's sensitivity for detecting positron-annihilation events occurring near the middle of the scanner in the axial direction is significantly higher than its sensitivity for detecting annihilations located near either end of the scanner. This is because many more detector rings are

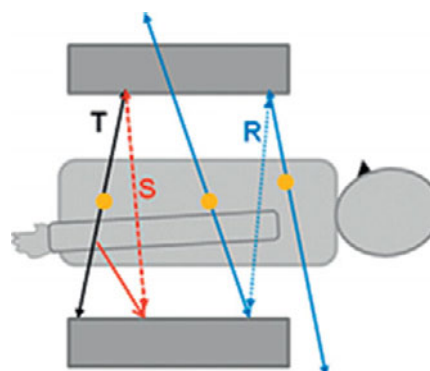


Figure 1.8 Three coincidence-event topologies: (black) a true coincidence, (red) a scattered coincidence, and (blue) a random coincidence. Dashed (dotted) lines represent incorrectly assigned LORs for scattered (random) coincidence events.

available for recording coincidences between back-to-back annihilation photons in the middle of the scanner than near its ends. In fact, at the extreme edges of the scanner's axial field-of-view (FOV), only one detector ring can acquire valid coincidence events. For event positions in between the center and the ends, the system coincidence sensitivity decreases linearly from its maximum value in the center to its lowest value at the end rings. On the other hand, in 2-D-mode imaging, the PET scanner's sensitivity is more constant along the axial direction. One important implication of the falloff in 3-D count sensitivity near the axial ends of the PET gantry is that a larger overlap between adjacent axial bed positions must be used for 3-D-mode imaging over multiple bed positions, in comparison with 2-D-mode PET, in order to better equalize the count sensitivity over the entire axial region being scanned. In practice, this means that if, for example, five 15-cm axial bed positions are sufficient to cover the torso region in a 2-D-mode whole-body scan, then seven bed positions might be required to achieve the same axial coverage in 3-D mode. Fortunately, however, because of the greater overall count sensitivity in 3-D mode, less acquisition time is needed for each bed position in 3-D than in 2-D, so a whole-body PET scan can still often be acquired in the same time, or even more rapidly, in 3-D mode than in 2-D mode.

Types of coincidence events; corrections for randoms and scatter

PET scanners acquire three different types of coincidence events, as illustrated in Figure 1.8. The most desirable event topology is a **true-coincidence** event, in which both photons

Chapter 1: PET and PET/CT physics, instrumentation, and artifacts

from one positron–electron annihilation are detected back-to-back along the correct LOR. Sometimes, however, one or both of the annihilation photons undergo Compton scattering in the patient before being detected. In this case, the **scatter-coincidence** event will appear to originate along an incorrect LOR. Finally, it is often possible for two annihilation photons originating from two *different* nuclear decays to be detected by chance within the coincidence time window, which will also lead to an incorrectly specified LOR; this type of event is called a **random coincidence**. Ideally, we would like to preserve all of the true-coincidence events, while rejecting all scatter- and random-coincidence events before reconstructing images; however, it is not possible to reject all of the “bad events” with current PET technology. By using detectors with improved performance characteristics, it is possible to reduce the number of detected scatter and random coincidences, but not to eliminate them completely. Fortunately, however, techniques have been developed to compensate for these sources of error while reconstructing PET images.

One can reduce the number of detected random-coincidence events by simply using a narrower coincidence time window; however, this approach will also reject more true-coincidence events because the timing resolution of the detectors is not perfect. By using fast scintillators, like some of those shown in Table 1.2, PET instrument designers are able to set narrower coincidence time windows in order to reduce the contribution of randoms to the PET coincidence data; however, the percentage of randoms in most whole-body PET studies is still, typically, 10–15% in 2-D mode, and 30–35% in 3-D mode, so correction for the random events is still required. One correction method is known as **delayed-window randoms subtraction**. With this approach, the PET scanner records two different types of coincidences. One type consists of all of the events described above which fall within the usual **prompt-coincidence** window; however, the scanner additionally can search for events detected in a **delayed window**; these consist of events in which the second photon is detected within a different time window that is set to be much later than the time when the first photon was detected. The time delay between the two detected photon events is chosen to be large enough so that a true- or scatter-coincidence event could never be detected in the delayed window; however, the LOR distribution of random coincidences in a delayed window is, statistically, the same as that observed in the prompt window. Although the delayed-window randoms approach provides accurate estimates of the rate of random coincidences along each LOR, these estimates are “noisy,” i.e., there can be a large variability of the estimates of the random-coincidence contribution to each LOR. For this reason, lower noise approaches have been devised; in one such method, the random-coincidence count-rate is computed from the so-called **single-event** count-rate on each detector (9). To use this **randoms-from-singles** method, the scanner’s electronics must be able to keep track of the total number of photons detected per second, which is the singles count-rate, in all of the

detector elements. For a coincidence time window width, τ , it can be shown that a good estimate of the expected random-coincidence count-rate, R , along any given LOR is then simply given by:

$$R = 2 \tau S_1 S_2,$$

where S_1 and S_2 are the singles count-rates recorded for the two detector elements defining the LOR.

Turning our attention now to the scatter-coincidence events, one way to reduce the number of these less desirable events would be, in principle, to use detectors with improved energy resolution. Because photons which undergo Compton scattering in the patient lose some energy in the process, if the detectors could measure a scattered photon’s energy with great accuracy, we should be able to reject more scattered events. However, even when using the brightest scintillation detectors shown in Table 1.2, the energy resolution of the detectors is not great, so a wide energy window must still be used in order to include most of the desirable true-coincidence events. The fraction of scattered photons detected within the scanner’s energy window is then still rather large, i.e., approximately 20–30% in 2-D mode, and 40–60% in 3-D mode.

Two general approaches have been developed to estimate the scattered-photon contribution to the projection data. One simple method, most often used for 2-D PET imaging, assumes that the scattered photon contribution can be estimated (after subtraction of random coincidences) by mathematically smoothing the coincidence-projection data using blurring functions which are measured using sources located at several different radial positions in a cylindrical phantom (10). Estimating the scatter data in 3-D-mode imaging is more challenging (11, 12); this is generally accomplished by starting from an initial estimate of the PET image, along with an attenuation map (e.g., obtained from CT), and then using these to compute the expected distribution of scatter-coincidence events; this calculation is based on the Klein–Nishina formula, which describes the angular distribution of Compton-scattered photons. Once the scattered-photon contribution to the raw data has been estimated, it can be used to refine the PET emission-image estimate, and the process could then be repeated in an iterative fashion until the estimated scatter contribution to the projection data no longer changes significantly.

Finally, we point out that there are two different general approaches to correcting for random and scatter coincidences. In one approach, the estimates of these “bad-coincidence” contributions are first subtracted from the measured projection data. Then, the remaining coincidence data, which would ideally represent only true-coincidence events at this point, can be reconstructed by one of several different tomographic reconstruction algorithms. There are a couple of possible problems with data-subtraction techniques. First, the subtracted projections could contain some negative values, for example, if the random or scatter contributions were overestimated, or if the projection data simply had too many statistical

Part I: General concepts of PET and PET/CT imaging

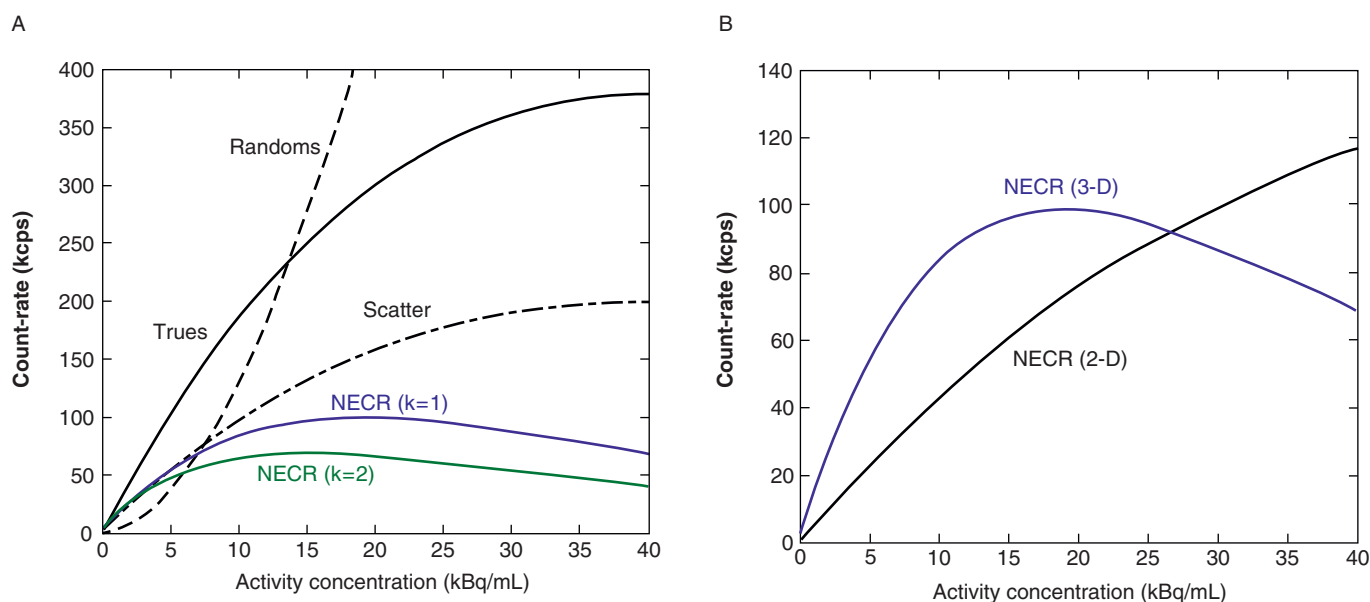


Figure 1.9 (A) Count-rates in 3-D mode vs. activity concentration; (B) noise-equivalent count-rate (NECR) curves for 3-D and 2-D mode scanning.

noise variations. While negative projection LOR values do not adversely affect some reconstruction algorithms, such as **filtered backprojection** methods, they can, however, cause serious problems for certain types of **iterative reconstruction algorithms**, which require that both the projection data and the reconstructed image be positive. Second, whenever one noisy data set is subtracted from another noisy data set, the relative statistical variability of the resulting data is significantly increased in comparison with the noise in the original data. Therefore, even if the subtraction approach is, on average, *unbiased*, or accurate, the subtraction technique is known to produce an amplification of the reconstructed PET image noise, which adversely affects overall image quality.

The other approach is to include the estimates of random and scatter coincidences *additively* when estimating the total projection data within an iterative reconstruction algorithm. In the popular **maximum-likelihood image reconstruction** methods (13) this approach provides an important advantage, because such methods rely on the assumption that the total projection data can be described by a joint Poisson statistical model of the counting noise in all of the detector elements. If the scatter and random coincidences are subtracted from the data, this assumption is violated, whereas if these “bad-coincidence” contributions are included additively, then the Poisson-statistics assumption can be preserved, which mitigates problems with excessive noise amplification during image reconstruction.

Noise-equivalent count-rate (NECR)

A useful approximate metric for assessing the deleterious effect of random and scatter coincidences on overall PET image quality is the so-called noise-equivalent count-rate (NECR) (14). NECR is the count-rate recorded by an *ideal* PET scanner

(i.e., a scanner that could perfectly reject all random and scatter coincidences) which would yield PET images with a noise level the same as that obtained from a *real* PET scanner after correcting for randoms and scatter. For a PET scanner recording true-coincidence rate, T , scatter-coincidence rate, S , and random-coincidence rate, R , the NECR is given by:

$$NECR = \frac{T^2}{(T + S + kR)}$$

In this formula, the multiplier “ k ” in the denominator is 2 when the delayed-window randoms subtraction method is used, or 1 when a very low-noise randoms estimate, e.g., the randoms-from-singles approach, is used.

3-D-mode count-rate curves are shown in Figure 1.9A as a function of the activity concentration within a phantom; these curves were measured for a modern PET scanner equipped with LYSO detector modules. (LYSO is similar to LSO, in terms of the basic properties listed in Table 1.2.) It can be seen that the true-coincidence count-rate initially increases linearly with activity concentration, until the system begins to lose events at high count-rates because of increasing detector “dead-time.” The scatter-coincidence count-rate is approximately half of the trues count-rate; the shapes of these curves are the same because a loss of counts at high rates due to detector dead-time influences the trues and scatters in the same way. The random-coincidence count-rate is initially much less than that of the true- and scatter-coincidences; however, the randoms rate increases rapidly, i.e., as the *square* of activity concentration, which causes the noise-equivalent count-rate (NECR) to increase to a maximum value (in this case, at an activity concentration of about 16–19 kBq/mL) and then to decrease with further increases in activity concentration. The maximum NECR for this scanner in 3-D mode